Supporting Information

Core-shell Covalent Organic Framework-Copper Nickel Disulfide Nanoreactors for the Synergistic Treatment of Wound Infections

Hongmei Deng[a+], Tongyao Wang[a+], Junlun Zhu[a+], Ziwei Xiang[a], Yuzhu Long[a], Yuzhu Yuan[a], Wei Wen[a], Shengfu Wang[a], Shaojiang Zheng[b]*, Xiuhua Zhang[a]*, Huayu Xiong[a]**

[a]: Ministry of Education Key Laboratory for the Synthesis and Application of Organic Functional Molecules, Collaborative Innovation Center for Advanced Organic Chemical Materials Co-constructed by the Province and Ministry, College of Chemistry and Chemical Engineering, Hubei University, Wuhan 430062, P. R. China..

[b]: Key Laboratory of Emergency and Trauma of Ministry of Education, Engineering Research Center for Hainan Biological Sample Resources of Major Diseases, the First Affiliated Hospital, Hainan Medical University, Haikou 570102, China.

[+]: These authors contributed equally to this work.

[*]: Corresponding authors.

E-mail: zshaojiang@muhn.edu.cn; zhangxh@hubu.edu.cn; xionghuayu@hubu.edu.cn

Contents

1. Experimental Materials and Methods

Materials. Sodium thiosulfate pentahydrate ($Na_2S_2O_3 \cdot 5H_2O$), reduced glutathione (GSH), nickel nitrate hexahydrate ($Ni(NO_3)_2 \cdot 6H_2O$), methoxy polyethylene glycol phosphatidylethanolamine (mPEG-DSPE), polypyrrolidone (PVP, wt 50000), 5,5'-dithiobis-(2-nitrobenzoic acid) (DTNB), glycol, hydrogen peroxide (H_2O_2), copper nitrate trihydrate ($Cu(NO_3)_2 \cdot 3H_2O$), o-nitrophenyl-β-D-galactopyranoside (ONPG), terephthalic acid (p-TA) and 3,3',5,5'-Tetramethylbenzidine (TMB) were purchased from Aladdin (Shanghai, China). Sodium acetate buffer solution (10 mM HAc-NaAc, pH 4.5) was purchased from Yuanye (Shanghai, China). Ethanol, acetonitrile, and acetic acid (HAc) were supplied by Sinopharm (Shanghai, China). 1,3,5-benzenetrialdehyde (M1) and 4,4',4''-(1,3,5-triazine-2,4,6-triyl)trianiline (M2) were from Jilin Institute of Chinese Academy of Sciences (Jilin, China). Calcein-Am and PI live-dead cell double-staining kits were provided by Solarbio (Beijing, China). The H_2O_2 detection assay Kit was commercially provided by Abcam (Shanghai, China). Other reagents (analytical grade) should be employed directly in the condition in which they were received. Deionized water (Mill-Q, Millipore) was used to prepare all solutions.

Characterization. Cu-NiS_2@COF@PEG nanoreactor uses energy-dispersive spectroscopy (EDS) to record the presence and distribution of elements. The bacterial morphology was examined using scanning electron microscopy (SEM, JSM7100F, Japan). The structure of Cu-NiS_2@COF@PEG nanoreactor was analyzed with a transmission electron microscope (TEM, CLY26G②20S-TWIN, FEI, USA). X-ray diffractograms (XRD) figures were obtained by operating the D8 Advance X-ray diffractometer (together with Cu Kα radiation, Bruke, Germany). An infrared spectrometer (Nicolet Is10, HGY02, Thermo, China) was used for the detection of Fourier transform infrared spectroscopy (FTIR). The elemental composition and valence state were tested via X-ray photoelectron spectroscopy (XPS, Escalab 250Xi). UV-Vis absorption spectra were obtained using UV-Vis-NIR spectrophotometer (Cary 6000iv, Agilent Corporation, USA) and UV spectrometer (UV-3600, Shimadzu

Corporation, Japan). A fluorescence spectrophotometer (RF-5301PC, Shimadzu, Japan) detected fluorescence signals. The Optimal 8000 inductively coupled plasma atomic emission spectrometer (ICP-AES) was used to monitor Cu and Ni ions release behavior of Cu-NiS_2@COF@PEG nanoreactor within 48 h. Fluorescence images of *Staphylococcus aureus* (*S. aureus*) were obtained by laser confocal scanning microscopy (CLSM, LSM 900, Zeiss, Germany).The contents of Cu and Ni in major organs were determined using an Agilent 7800 inductively coupled plasma mass spectrometer (ICP-MS, Agilent Technologies, USA). The specific surface areas of COF and Cu-NiS_2@COF were determined via the Brunauer-Emmett-Teller (BET) method using a Micromeritics ASAP 2460 physical adsorption analyzer (Micromeritics Corporation, USA).

Fabrication and performance evaluation of Cu-NiS_2@COF@PEG nanoreactor.

Synthesis of Cu-NiS_2. Cu-NiS_2 was prepared using an improved solvothermal method.[1] Briefly, $Ni(NO_3)_2 \cdot 6H_2O$ (1 mmol), $Na_2S_2O_3 \cdot 5H_2O$ (3 mmol), PVP (0.3 g), and $Cu(NO_3)_2 \cdot 3H_2O$ (0.25 mmol) were mixed in a solution containing glycol (40 mL) and deionized water (40 mL), stirred magnetically for 4 h after completely dissolving, followed by reaction in an autoclave at at 180 ℃ for 12 h. A centrifugal cycle with ethanol was performed 3 times (1000 rpm/min, 10 min), followed by vacuum desiccation at 60 ℃ over a 10 h interval to yield the target material.

Synthesis of Cu-NiS_2@COF. Cu-NiS_2@COF is based on the literature with some modifications.[2] Cu-NiS_2 (14.0 mg) and M2 (14.2 mg) were dissolved and dispersed in 3 mL of acetonitrile in glass bottles. After 1 h of ultrasound treatment, the reaction system was subjected to the addition of M1 (6.5 mg) in a 2 mL acetonitrile mixture. After ultrasonic treatment for 30 min, 0.4 mL of HAc (12 M) was added to this solution. 40 % power ultrasonic treatment was applied for 2 h, followed by magnetic stirring for 5 h. Wash the final filtered yellow solid with ethanol and then dry to give Cu-NiS_2@COF.

Fabrication of Cu-NiS_2@COF@PEG nanoreactor. Cu-NiS_2@COF (10 mg) was evenly dispersed in 5 mL of deionized water, and mPEG-DSPE (1 mg/mL) dissolved in advance was added, stirred for 4 h, and the precipitate was collected. A

centrifugation washing cycle was performed at 1000 rpm/min for 3 times. The final obtained Cu-NiS_2@COF@PEG nanoreactor was freeze-dried and then dispersed in phosphate buffer (PBS) to facilitate the follow-up experiment.

Evaluation of catalytic performance. POD-like properties of Cu-NiS_2@COF@PEG nanoreactor were examined with TMB probe, and then the reaction was performed with or without H_2O_2 (0.1 mM) in 3 ml PBS (0.1 M, pH=5.0), including Cu-NiS_2@COF@PEG (150 μg/mL) and TMB (1.0 mM) under oxygen (O_2) saturation, nitrogen (N_2) saturation, or air conditions. The mixture solutions were maintained under thermostatic conditions (37°C) for an incubation of 7 min; color development results were photographed and tested using UV-Vis absorption spectroscopy. P-TA functioned as a fluorescent probe to assess the capacity of Cu-NiS_2@COF@PEG nanoreactor's capacity to generate ·OH through catalytic reaction with H_2O_2. A mixture solution of 150 μg/mL Cu-NiS_2@COF@PEG and 0.5 mM p-TA was prepared. After incubation for 5 min with or without hydrogen peroxide (0.1 mM), the fluorescent signal was detected at 425 nm (λ_{ex}=315 nm). At N_2 saturation, a variety of TMB concentrations were tested alongside an excess of H_2O_2 (30 mM), or alternatively, different concentrations of H_2O_2 with a surplus of TMB (30 mM). The apparent steady-state kinetic analysis of Cu-NiS_2 nanozymes with POD-like activity was performed at O_2 saturation and at different concentrations of TMB.

Use DTNB as a probe to assess GSH consumption. A mixed solution was prepared with 1 mM of GSH and 150 μg/mL of Cu-NiS_2@COF@PEG. The samples were subjected to a thermostatic temperature shaker, maintained at 37 °C with a rotational speed of 150 rpm, and measured at intervals of every thirty minutes. 0.9 mL (0.1 mM) of DTNB was combined with 0.1 mL of the sample at each time point, and the absorption spectrum was tested with UV-Vis. To illustrate GSHOx-like activity of nanozymes, the product was detected using an H_2O_2 kit. Incubate 150 μg/mL of Cu-NiS_2 nanozyme or Cu-NiS_2@COF@PEG nanoreactor with a mixture of 1.0 mM GSH for 1 h at room temperature. Then measure by UV-Vis absorption spectrum.

Study on photothermal properties of Cu-NiS_2@COF@PEG nanoreactor. The photothermal properties of PBS and Cu-NiS_2@COF@PEG nanoreactors at various concentrations (50, 100, 150, 200 μg/mL) were evaluated using an 808 nm NIR laser

at a power density of 1.0 W/cm^2. The 150 μg/mL Cu-NiS_2@COF@PEG nanoreactor was irradiated with lasers at varying powers (0.8, 1.0, 1.2 W/cm^2). The photothermal stability of the Cu-NiS_2@COF@PEG nanoreactor (150 μg/mL) was evaluated through five laser on/off cycles. In the above experiments, an infrared thermographer (Testo, Germany) was used to obtain real-time thermal images and temperature rise values. The photothermal conversion efficiency (η) of Cu-NiS_2@COF@PEG nanoreactor was calculated according to the reference.[3]

Antibacterial activity assay of Cu-NiS_2@COF@PEG nanoreactor *in vitro*. *S. aureus* was used as the model bacterium in the antibacterial assay, which was divided into six groups to experiment: (a) control; (b) Cu-NiS_2@COF@PEG nanoreactor; (c) Cu-NiS_2@COF@PEG nanoreactor + H_2O_2; (d) Cu-NiS_2@COF@PEG nanoreactor + NIR; (e) Cu-NiS_2@COF@PEG nanoreactor + H_2O_2 + NIR; (f) Cu-NiS_2@COF@PEG nanoreactor + H_2O_2 + NIR + glucose. Group f simulated hyperglycemia. 1 mL of fresh Luria-Bertani (LB) medium was used to inoculate with 0.1 mL of logarithmic phase bacterial cells (~10^9 CFU/mL). Under various conditions of treatment, including PBS, 150 μg/mL of Cu-NiS_2@COF@PEG nanoreactor, 0.1 mM of H_2O_2, irradiation with an 808 nm NIR laser with a power density of 1.0 W/cm^2 for 5 min at 55 °C, or treatment with a glucose concentration of 5 mg/mL, each group was cultured at 37 °C for 12 h. LB solid medium was inoculated by the smear method and cultured at 37 °C for a period of 12 h, and colony counts were determined using the plate counting method. The washed bacterial solution was fixed with 2.5 % glutaraldehyde, then eluted with an ethanol gradient of varying concentrations before bacterial morphology was observed via SEM. Antibacterial rates were calculated according to the reference.[4]

Biofilms were incubated in 6-well plates under different conditions for 48 h, then washed with PBS, replenished with fresh medium, and co-stained with NucGreen and EthD-III (Solarbio, Beijing, China) for 15min. Biofilms were observed via CLSM: green fluorescence indicated intact biofilms, and red fluorescence indicated damaged biofilms.

Cell proliferation and migration. Human umbilical vein endothelial cells (HUVECs)

were inoculated into 96-well plates at a density of 10^5 cells/well and cultured in HAM's F-12 medium (Wuhan Punosai Biotechnology Co., LTD.). The medium contained 10 % fetal bovine serum (Gibco), 0.03 mg/mL ECGS (MultiSciences Biotech Co., Ltd.), 1 % penicillin-streptomycin (Gibco), and 0.1 mg/mL heparin (Biosharp). After 24 h of culture, the cells were further incubated in a conditioned medium (containing 150 μg/mL Cu-NiS_2@COF@PEG nanoreactor) for 24 or 48 h, and cell proliferation was assessed using the methylthiazolyldiphenyl-tetrazolium bromide (MTT) method.

Cell migration behavior was evaluated using Transwell inserts (8.0 μm). The basal compartment was supplemented with 1 mL of conditioned medium, whereas 1.5×10^4 cells were seeded in the apical chamber. After 3 days, the cells remaining in the apical chamber were carefully removed, and those that migrated to the basal compartment were stained with crystal violet. In the cell live/dead assay, mouse fibroblast cells (NIH-3T3) were plated in 6-well culture plates at a density of 1×10^6 cells/well. After 24 h of culture, the medium was replaced with conditioned medium containing nanoreactors, and the cells were incubated for another 24 h. Subsequently, Calcein-AM and PI staining were used to distinguish live cells from dead cells.

Hemolysis tests. The rat whole abdominal aortic blood was mixed with anticoagulant, washed with PBS (pH 7.4), and centrifuged 3 times (3000 rpm, 15 min) at 4 °C. 900 μL of H_2O, PBS, or Cu-NiS_2@COF@PEG nanoreactor solutions at various concentrations were mixed with 100 μL of blood to a final volume of 1000 μL blood mixture. The mixture was incubated in a 37 °C shaker (200 rpm) for 4 h, then centrifuged and photographed. UV-Vis absorption spectrum at 450-650 nm was detected using 0.5 mL of the supernatant.

Wound healing *in vivo* experiments. All animal experiments were executed in strict accordance with the guidelines approved by the Animal Ethics and Welfare Committee at Hubei University (registration number: 20220044). All the rats were male Sprague-Dawley (SD) rats aged six to eight weeks; they were taken from the Disease Control and Prevention (Wuhan, China). Four groups of experiments were designed: (a)control; (b) COF; (c) Cu-NiS_2@COF@PEG nanoreactor; and (d) Cu-

NiS_2@COF@PEG nanoreactor + NIR groups (n=6). Diabetes in rats was induced via a single intraperitoneal injection of approximately 60 mg/mL streptozotocin (STZ, Sigma) administered following a 12 h fast. After 3 days, rats exhibiting fasting blood glucose levels surpassing 16.8 mmol/L were measured with a glucose meter (Omron) for further study.

The wound infection model was established by incising a 15-mm wound on the dorsal skin of rats and then dropping 0.1 mL of *S. aureus* suspension (1.0×10^7 CFU/mL) onto the wound. 200 μL of PBS, COF suspension, or Cu-NiS_2@COF@PEG nanoreactor suspension was sprayed onto the wound surface, respectively; NIR laser exposure was administered to Group d. The temperature rise of Group d was recorded using an infrared thermograph 5 min after the wound was exposed to NIR light (1.0 W/cm^2) for treatment. Photos taken on days 1, 3, 7, 11, and 15 were used to observe changes in wound size, and quantification was performed using ImageJ software (LOCI). The wound healing rates were calculated based on the literature.[5] On day 7, the wound skin tissue was fixed in a 10 % paraformaldehyde solution. The sections underwent Masson's trichrome and hematoxylin-eosin (H&E) staining, and immunohistochemical analysis was performed to detect platelet endothelial cell adhesion molecule-1(CD31), Ki67 positive staining number, and VEGF. At the end of the experiment, aortic blood samples were collected for routine blood biochemical testing. Biological indicators, including creatinine (CREA), serum total protein (TP), aspartate aminotransferase (AST), alanine aminotransferase (ALT), uric acid (UA), and urea (UR), were measured. Subsequently, the rats were euthanized, and H&E staining was performed on major organs (heart, liver, spleen, lung, and kidney). Histological images were observed using a light microscope (CX-31, Olympus, Japan).

Statistical analysis. Mean ± standard deviation was used to represent the results. Group comparisons were conducted using a t-test. Differences were deemed statistically significant at $P < 0.05$ (*), 0.01 (**), or 0.001 (***).

2. Supporting figures

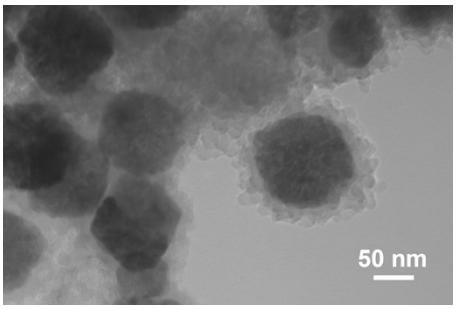

Fig. S1 TEM image of Cu-NiS_2@COF.

TEM images show Cu-NiS_2@COF with a particle size of approximately 220 ± 35 nm.

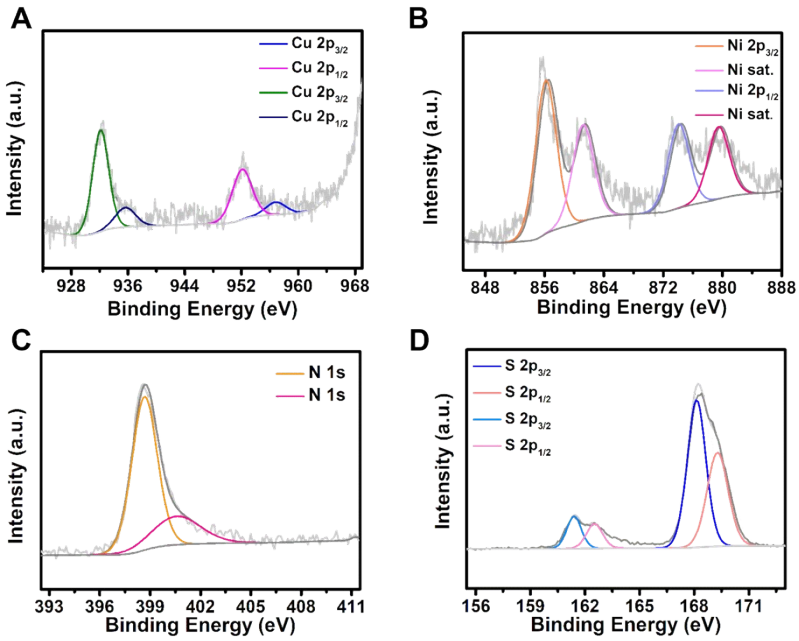

Fig. S2 XPS spectra of A) Cu 2_p, B) Ni 2_P, C) N 1_S, and D) S 2_P at Cu-NiS_2@COF@PEG nanoreactor.

The characteristic peaks (Fig. S2A) at 936.0 and 958 eV exhibited Cu $2p_{3/2}$, while 932.0 and 952.0 eV exhibited Cu $2p_{1/2}$, which were the binding energies generated by the successful doping of Cu in NiS_2.[6] The peaks (Fig. S2B) at 161.0 and 168.0 eV belonged to S $2p_{3/2}$, while 163.0 and 170.0 eV corresponded to S $2p_{1/2}$.[7] Characteristic peaks at 399.0 and 401.0 eV could be attributed to N 1s (Fig. S2C). The peaks (Fig. S2D) at 865.0 and 874.0 eV correspond to Ni $2p_{3/2}$ and Ni $2p_{1/2}$, respectively.[8,9] Characteristic peaks at 399.0 and 401.0 eV could be attributed to N 1s.

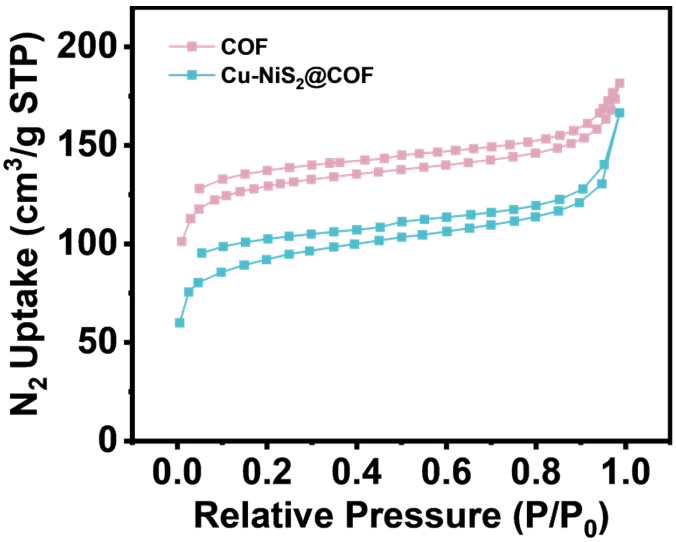

Fig. S3 N_2 adsorption and desorption isotherms of COF and Cu-NiS_2@COF at 77 K.

BET specific surface area of COF reaches 488.57 m^2/g, corresponding to the higher N_2 adsorption capacity in the figure, which indicates that it possesses an abundant mesoporous structure (characteristic of Type-IV isotherm) and can provide sufficient channel space for mass transport. In contrast, the specific surface area of Cu-NiS_2@COF decreases to 328.59 m^2/g with a synchronous reduction in adsorption capacity, demonstrating that Cu-NiS_2 nanozyme are successfully loaded and occupy part of COF channels. Nevertheless, the composite material still retains a relatively high porosity, which can maintain effective mass transfer capability.

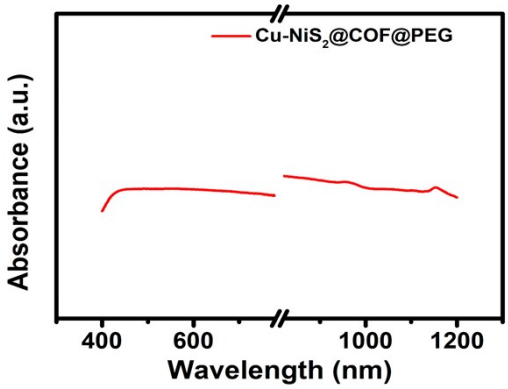

Fig. S4 UV-Vis absorption spectra of Cu-NiS_2@COF@PEG nanoreactor.

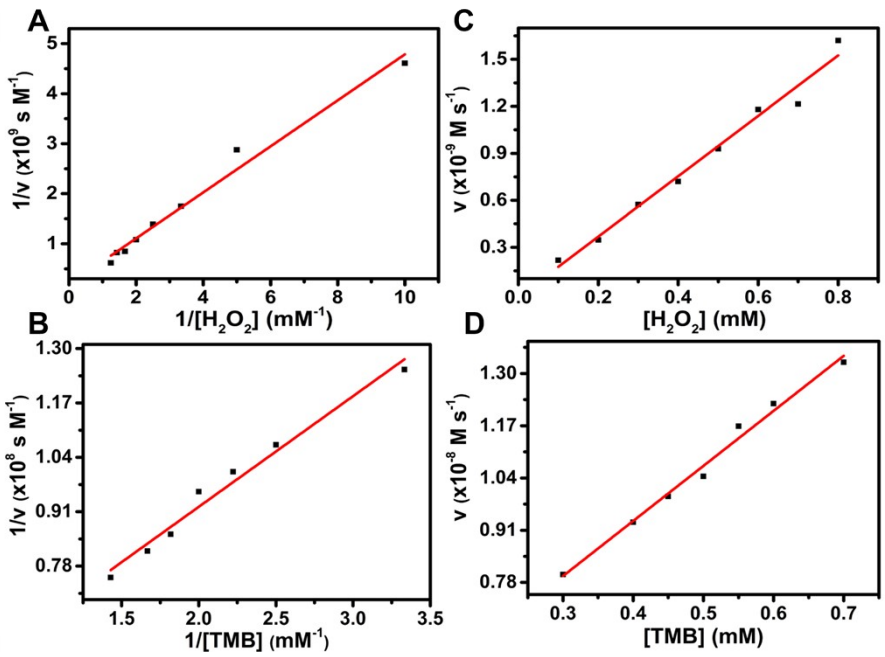

Fig. S5 Steady-state kinetics analysis of Cu-NiS_2 simulated POD-like. 0.2 mg/mL Cu-NiS_2 of 40 μL was added to 0.1 M PBS buffer containing different concentrations of H_2O_2 (pH=5.0), and the reaction rate of the system was determined under N_2 saturation conditions. A) When the concentration of TMB is 30 mM, change the concentration of H_2O_2. B) When the concentration of H_2O_2 is 30 mM, TMB concentration is different. C) and D) double reciprocal plots are used to determine the kinetic constants of Cu-NiS_2 for different substrates.

Kinetic parameters calculated by Lineweaver-Burk analysis show that when TMB is used as a substrate, the Michaelis constant (K_m) is 0.743 mM and the maximum velocity (V_{max}) is 2.59×10^{-8} M·s^{-1}. For H_2O_2 as a substrate, the corresponding values are 0.241 mM and 5.79×10^{-8} M·s^{-1}, respectively.

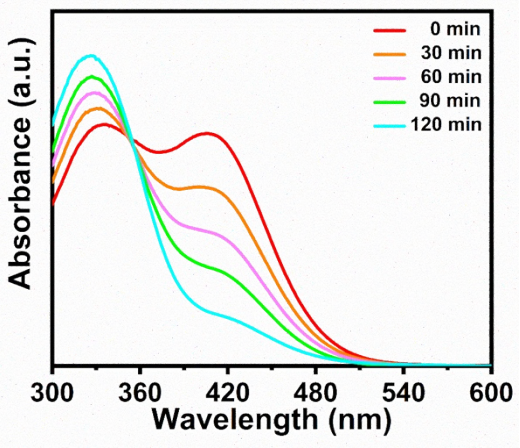

Fig. S6 Time-dependent UV-Vis absorption spectra of Cu-NiS_2@COF@PEG nanoreactor for GSH depletion using DTNB as probe

As shown in the spectrum at different time points, GSH concentration decreases with the incubation time of Cu-NiS_2@COF@PEG nanoreactor. When the incubation time reaches 120 min, the measured GSH concentration is the lowest.

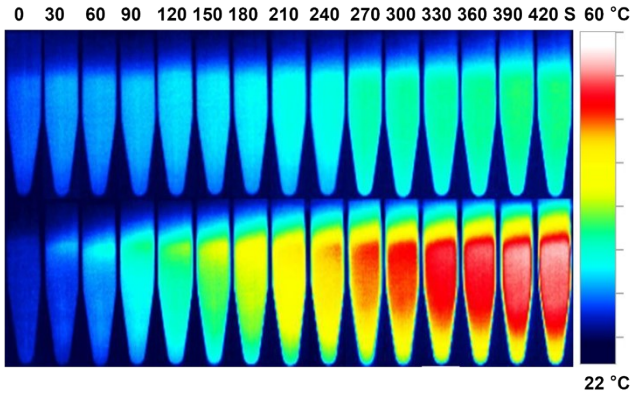

Fig. S7 Comparative infrared photothermal imaging of PBS (top) and Cu-NiS_2@COF@PEG nanoreactor (bottom) under 1.0 W/cm^2 NIR irradiation.

Higher laser density compared to PBS causes Cu-NiS_2@COF@PEG nanoreactor environment to heat up faster.

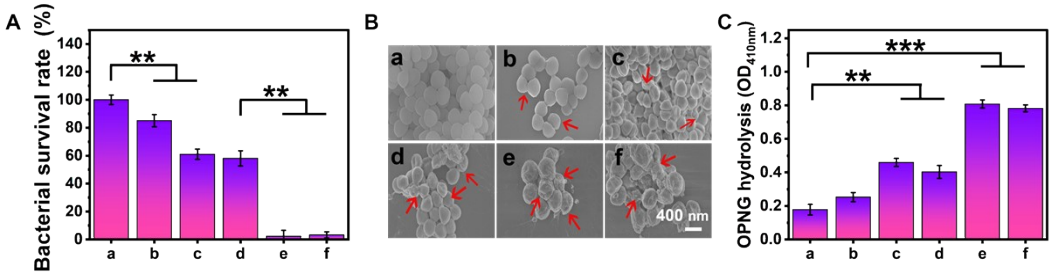

Fig. S8 A) Statistics of bacterial survival. B) SEM images of *S. aureus* after different treatments. C) ONPG hydrolysis degree of *S. aureus* after different treatments. a) PBS, b) Cu-NiS_2@COF@PEG nanoreactor, c) Cu-NiS_2@COF@PEG nanoreactor + H_2O_2, d) Cu-NiS_2@COF@PEG nanoreactor + NIR, e) Cu-NiS_2@COF@PEG nanoreactor + H_2O_2 + NIR and f) Cu-NiS_2@COF@PEG nanoreactor + H_2O_2 + NIR + glucose

In Fig. S8A, it can be clearly observed that without NIR irradiation, the bacterial survival rate in Group c was significantly lower than that in Groups a and b (even though all groups contained nanoreactors). When NIR irradiation was applied, the bacterial survival rate remained very low, even in the presence of glucose. Fig. S8B shows SEM images of bacteria with significant morphological alterations—including collapsed surfaces, pronounced distortion, and damaged membranes—in the synergistic treatment groups. In contrast, bacterial cells in the control group had smooth, intact cell membranes. Fig. S8C shows that the optical density (OD_{410}) values of Cu-NiS_2@COF@PEG nanoreactor treatment group were significantly higher.

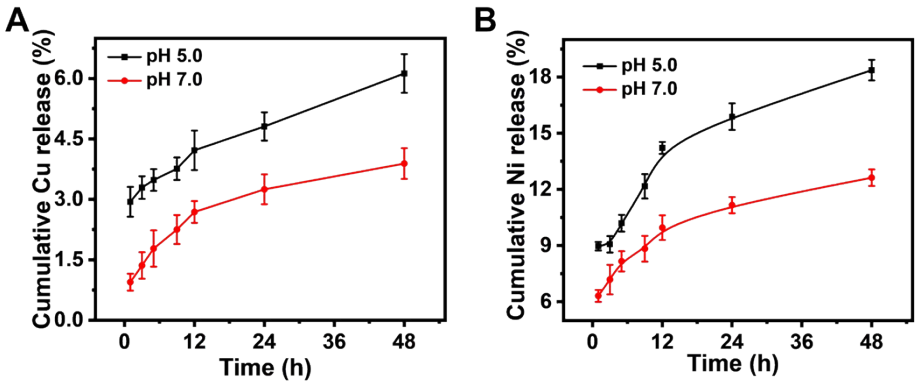

Fig. S9 The release processes of A) Cu and B) Ni in PBS with different pH.

The release of Cu and Ni ions was rapid in the first 12 h and then slowed down. Specifically, the cumulative concentration of released metal ions under acidic conditions was higher than that under neutral conditions.

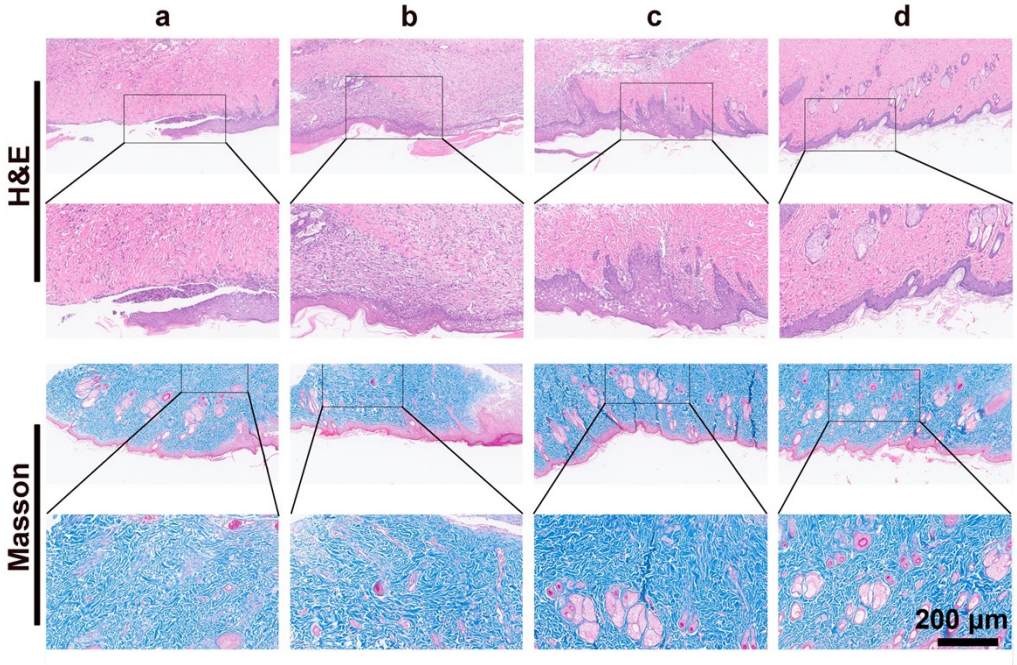

Fig. S10 H&E staining pattern and Masson staining pattern of the wound skins after treatments for 15 days. a) PBS, b) COF, c) Cu-NiS_2@COF@PEG nanoreactor, d) Cu-NiS_2@COF@PEG nanoreactor + NIR

The results showed increased epithelial thickness, as well as the regeneration of sebaceous glands and hair follicles, indicating the potential wound-healing efficacy of Cu-NiS_2@COF@PEG nanoreactor under light exposure.

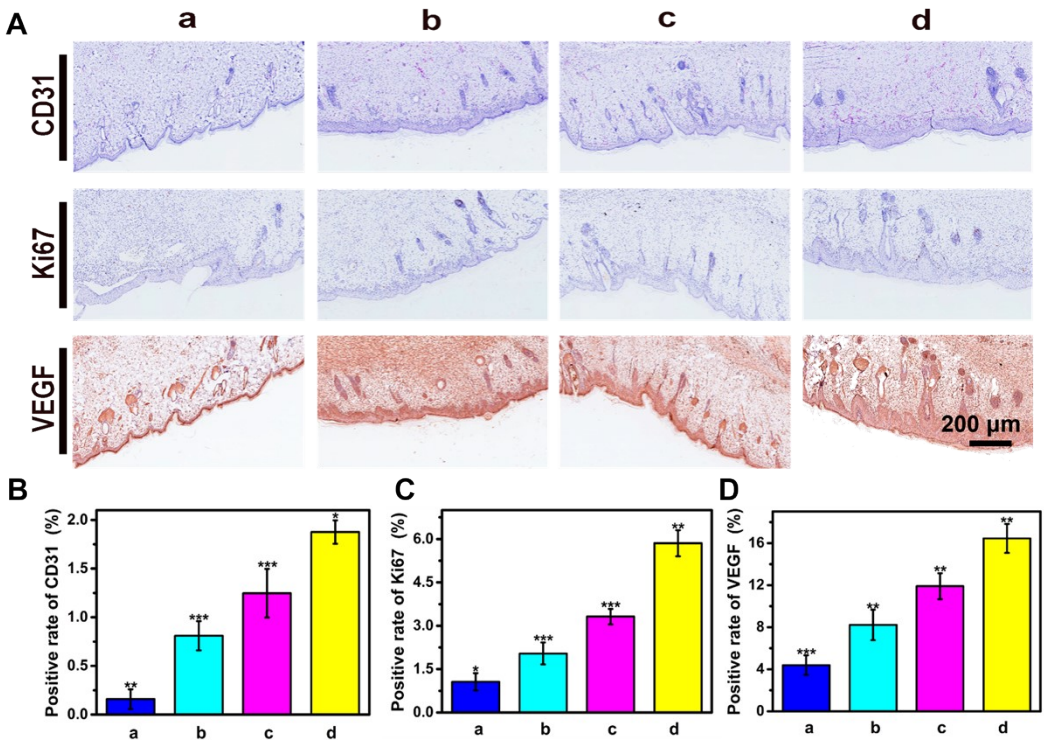

Fig. S11 A) Immunohistochemical staining images of CD31, Ki67, and VEGF on day 7. The quantitative results of B) CD31, C) Ki67, and D) VEGF by the Image J software. **p < 0.01, ***p < 0.001.

As shown in Fig. S8, the positive staining indices of CD31, Ki67, and VEGF in the combined treatment group were significantly higher than those in the control group.

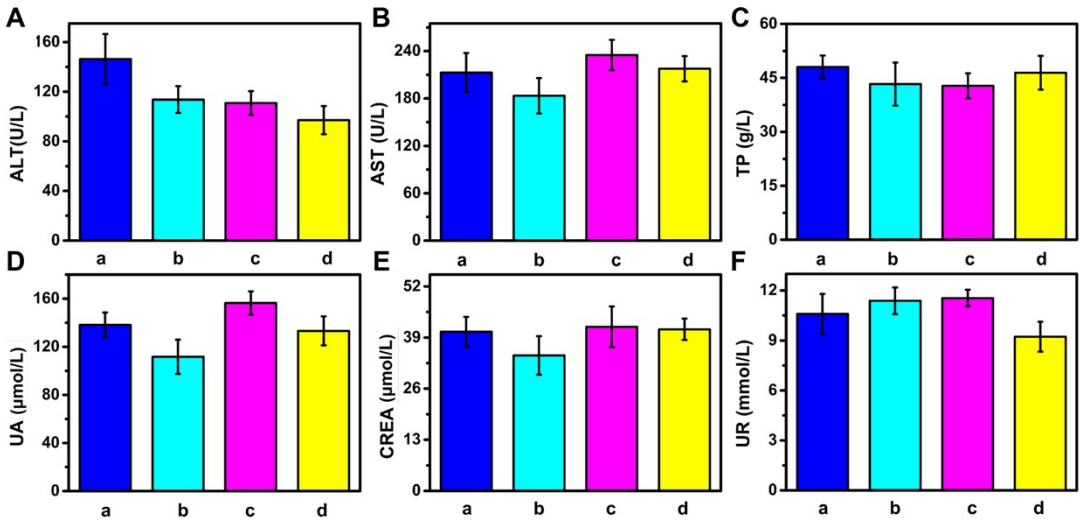

Fig. S12 (A-F) Blood biochemical values of rats after treatment for 15 days.

The results of blood biochemical tests, including ALT, AST, TP, UA, CREA, and UR, are listed in Fig. S9; all parameters are within normal limits.

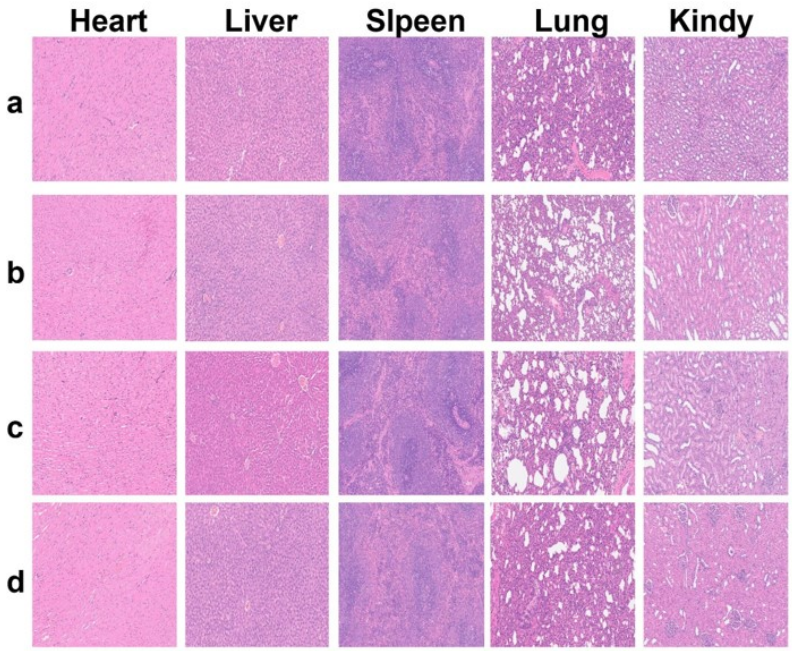

Fig. S13 Images of H&E-stained tissue slices of major organs (heart, liver, spleen, lung, and kidney) of rats after 15 days of treatment with different treatments.

In comparison with the control group, no signs of abnormality or inflammatory response were detected in the stained tissue sections of the treated rats' major organs, including the heart, liver, spleen, lung, and kidney.

3. Supporting table

Table S1. Comparison of nanozyme the kinetic parameters in different catalysts.

Catalyst	K_m (mM)		V_{max} (10^{-8} M·s^{-1})		Reference
	TMB	H_2O_2	TMB	H_2O_2	
Cu-NiS_2	0.743	0.241	2.59×10^{-8}	5.79×10^{-8}	This work
CuS	0.409	0.406	6.32×10^{-8}	5.49×10^{-8}	10
Fe_3O_4	0.098	154	3.44×10^{-8}	9.78×10^{-8}	11

According to Table S1, K_m value of Cu-NiS_2 nanozyme for H_2O_2 is 0.241 mM, which is lower than that of CuS and Fe_3O_4 nanozymes. This indicates that Cu-NiS_2 nanozyme has a higher affinity for H_2O_2. Meanwhile, V_{max} value of Cu-NiS_2 nanozyme is 5.79×10^{-8} M·s^{-1}, which is comparable to that of CuS nanozyme and higher than that of Fe_3O_4 nanozyme. This demonstrates that Cu-NiS_2 nanozyme possesses a favorable catalytic capability.

Table S2. Cu and Ni content in major organs (liver, spleen, and kidney) after 14 days of treatment.

Metal	Group	Organs metal level		
		Liver	Spleen	Kidney
		μg/metal/g wet wt		
Cu	Control	15.23 ± 0.99	2.36 ± 0.16	3.92 ± 0.64
	Cu-NiS_2@COF@PEG	16.35 ± 1.14	2.39 ± 0.28	4.36 ± 0.46
Ni	Control	0.35 ± 0.08	0.11 ± 0.04	0.20 ± 0.07
	Cu-NiS_2@COF@PEG	0.39 ± 0.07	0.10 ± 0.02	0.19 ± 0.01

Following treatment with Cu-NiS_2@COF@PEG nanoreactors, the contents of Cu and Ni in major organs did not deviate from the physiological levels of the control group. This result indicates that the nanoreactors did not induce abnormal accumulation of Cur and Ni in major organs, thereby verifying their biosafety.

References

1. G. He, Y. Ma, H. Zhou, *et al*., J. Mater. Chem. B., 2019, **7**, 143-149.
2. Y. Wang, Z. Hu, W. Wang, *et al*., *Chem. Sci.*, 2021, **12**, 16065-16073.
3. Z. Y. Jiang, C. L. Zhang, X. Q. Wang, *et al*., *Angew. Chem. Int. Ed.*, 2021, **60**, 22376-22384.
4. Y. Deng, X. M. Ouyang, J. Y. Sun, *et al*., *Bioact. Mater.*, 2023, **25**, 748-765.
5. Y. D. Ma, X. Y. Lai, X. Luo, *et al*., *Adv. Funct. Mater.*, 2024, **34**, 2405644.
6. K. N. Dinh, Y. X. Sun, Z. X. Pei, *et al*., *Small*, 2020, **16**, 1905885.
7. Y. M. Lin, Z. Z. Qiu, D. Z. Li, S. *et al*., *Energy Storage Mater.*, 2018, **11**, 67-74.
8. F. L. Zhang, H. M. Hao, X. Y. Dong, *et al.*, *Appl. Catal. B.*, 2022, **305**, 121027.
9. Y. C. Wang, D. L. Chao, Z. Z. Wang, *et al*., *Acs Nano*, 2021, **15**, 5420-5427.
10. Y. J. Zhang, S. Q. Yang, J. Wang, *et al*., *Talanta*, 2021, **233**.
11. L. Z. Gao, J. Zhuang, L. Nie, *et al*., *Nat. Nanotechnol.*, 2007, **2**, 577-583.